Received: 15 February 2024 | Revised: 16 April 2024 | Accepted: 17 April 2024

DOI: 10.1002/jrs.6675

RESEARCH ARTICLE

Journal of RAMAN SPECTROSCOPY WILEY

Raman spectroscopy, phase transitions, microstructures, and mechano-luminescence in Ca-Sr feldspars ($CaAl_2Si_2O_8$-$SrAl_2Si_2O_8$)

Nadia Curetti | **Davide Bernasconi** | **Mario Tribaudino**

Department of Earth Sciences, University of Torino, Turin, Italy

Correspondence
Mario Tribaudino, Department of Earth Sciences, University of Torino, Via Valperga Caluso, 35, I-10125 Turin, Italy.
Email: mario.tribaudino@unito.it

Funding information
This work was supported by TRIM_AUTOF_23_01 self-supported research funding from the University of Torino to Mario Tribaudino.

Abstract

The Raman spectra of $Ca_{1-x}Sr_xAl_2Si_2O_8$ ($0 \leq x \leq 1$) feldspars have been measured, to investigate at a short-range scale the effect of changing composition on the $P\bar{1} \rightarrow I\bar{1}$ and $I\bar{1} \rightarrow I2/c$ phase transitions and how phase transitions affect the mechano-luminescence found in these feldspars. Transmission electron microscopy (TEM) and X-ray diffraction (XRD) were done on the same samples, to pinpoint the transitions, by the analysis of selected area diffraction patterns (SAED) and of the spontaneous strain. Natural anorthite ($CaAl_2Si_2O_8$) shows a large number of well-resolved peaks, together with sharp h + k even, l odd diffractions (*c*-type) in SAED patterns, indicative of a $P\bar{1}$ symmetry. In synthetic anorthite, the Raman spectrum is similar to that of natural anorthite, but the peaks are broader, and c-type reflections are elongated. As Sr increases, the *c*-type reflections become more diffuse and elongated, as the Raman peaks do. At $x > 0.6$, new peaks appear in Raman spectra, and other peaks show a change in their wavenumber. Moreover, the *c*-type reflections disappear completely, and the lattice becomes *I*-centred. Between $x \sim 0.6$ and $x = 0.86(3)$, the XRD patterns prompt for a triclinic structure, with S.G. $I\bar{1}$. The transition to the monoclinic $I2/c$ structure is well constrained by the ferroelastic strain, whereas the Raman spectra are more similar between the monoclinic and triclinic $I\bar{1}$ and $I2/c$ than between $I\bar{1}$ and $P\bar{1}$. The absence of mechano-luminescence in triclinic $I\bar{1}$ compositions suggests that this property is enhanced in local $P\bar{1}$ configurations at conditions close to the $P\bar{1}$ to $I\bar{1}$ transition. A possible mechanism for mechano-luminescence involving a compression induced $P\bar{1}$ to $I\bar{1}$ transition in local Eu^{2+} bearing $P\bar{1}$ configurations is proposed.

KEYWORDS
anorthite, mechano-luminescence, microstructures, phase transitions, Sr-feldspar

1 | INTRODUCTION

Feldspars are important phases in Earth Sciences, being the most common mineral family in the Earth crust. Feldspars are also a key phase in ceramics, and, in general, a major player in the high temperature processes involving alumina-silicates.

The general formula of feldspars is MT_4O_8, being T a tetrahedrally coordinated cation, and M an interstitial 8–9 coordinated one. In natural feldspars, the tetrahedral cation is Si or Al, and the M cation is Ca, Ba, Na or K. In synthetic analogues, also tetrahedrally coordinated Ga, B and Zn may exchange for Al, Ge for Si and Rb, Sr and Pb for the M cation.[1–3] The Si:Al ratio can vary between 3:1, in $NaAlSi_3O_8$ (albite) and $KAlSi_3O_8$ (K-feldspar), and 1:1 in $CaAl_2Si_2O_8$ (anorthite) and $BaAl_2Si_2O_8$ (celsian). Natural feldspars are solid solutions of albite and K-feldspar, and of albite and anorthite, forming the alkali-feldspar and plagioclase minerals. Also celsian occurs in nature, but in more restricted environments.[4]

The synthetic feldspar with the M site fully occupied by Sr is named Sr-feldspar ($SrAl_2Si_2O_8$). Between Sr-feldspar and anorthite, complete solid solution exists, in Ca-Sr feldspars. Synthetic Ca-Sr feldspars have been widely studied as a model for the behaviour of natural feldspars, but more recently also for their properties as materials and as host for environmentally toxic elements.

Sr-feldspar is monoclinic with *I*2/*c* S.G., whereas anorthite is triclinic with S.G. $P\bar{1}$ (Figure 1). Transitions between the monoclinic and triclinic symmetry occur with composition but are also induced by changing pressure and temperature. They were the subject of extensive research.[5–13]

Other studies investigated Sr-feldspar as a host for Sr^{85} radionuclide immobilization[14,15] and in fibre-reinforced glass–ceramic matrix composite ceramics.[16,17]

Most recently, the luminescence properties of Ca-Sr feldspars doped with REE were subject of interest. Doping of Eu^{2+} in the structure of Ca, Sr and Ba feldspars induced photoluminescence and pronounced phosphorescence, with longer afterglow in anorthite.[18] Further investigation showed that photoluminescence occurs also by doping with Mn^{2+}, Dy^{3+}, Pr^{3+}, Ce^{3+}, Tb^{3+} and Sm^{3+} together or without Eu^{2+} and Eu^{3+}.[19–24]

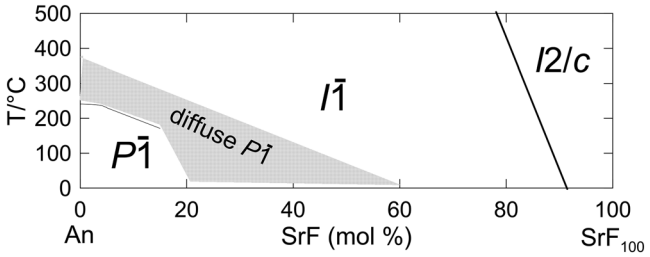

FIGURE 1 Phase diagram of $Ca_{1-x}Sr_xAl_2Si_2O_8$ feldspars; drawn from literature.[5,6]

Another interesting property of anorthite doped with Eu^{2+} is mechano-luminescence, first observed by Zhang et al.[25] Mechano-luminescence is luminescence activated by stress. It is found in a number of inorganic compounds,[26] but Eu doped anorthite is one of a few systems that have strong mechano-luminescence and blue-purple light. The mechano-luminescence emission can be enhanced by exchange of Sr for Ca in $Ca_xSr_{1-x}Al_2Si_2O_8$ feldspars: In $Ca_{0.6}Sr_{0.4}Al_2Si_2O_8$, the emission is up to three times that of Sr-free anorthite. However, for higher Sr exchange, at $Ca_{0.2}Sr_{0.8}Al_2Si_2O_8$, no mechano-luminescence is observed.[27–29] Feng et al.[29] interpreted this behaviour to be related to phase transitions, being mechano-luminescence more sensitive to the transition from a $P\bar{1}$ to $I\bar{1}$ structure, whereas photoluminescence and thermo-luminescence are affected by the $I\bar{1}$ to *I*2/*c* transition.

Among the different approaches able to characterize phase/structural transitions in solids, Raman spectroscopy can be particularly useful. Analysis of Raman spectra can detail the structural deformations and phase transitions in solid solutions, here involving Sr/Ca substitution, thanks to the position and intensity of specific vibrational bands. Moreover, the intrinsic local nature of Raman spectroscopy can be useful to probe at a local scale phase transition and how they are related to microstructures and physical properties like mechano-luminescence. Indeed, it provides information to map the phase distribution and, potentially, to obtain simultaneously the Raman and the photoluminescence spectrum in small amount dispersed in the ceramics or in synthetic products.[30]

For these reasons, in this study, we report the Raman spectra of a series of synthetic feldspars with composition $Ca_xSr_{1-x}Al_2Si_2O_8$, (anorthite-Sr feldspar, An-SrF, $CaAl_2Si_2O_8$-$SrAl_2Si_2O_8$) and x between 0 and 1, coupled with XRPD and SEM-EDS analysis. The spectroscopic data are discussed by taking also advantage of the results in previous TEM and high temperature XRD studies.[5,6,9–12] The phase transitions at short and long-range scale, together with the microstructure in intermediate Ca-Sr feldspars, will be discussed, with the aim to interpret the mechano-luminescence behaviour of these phases with composition.

2 | MATERIALS AND METHODS

The samples were obtained in previous investigations[5,6,9–12] by high temperature synthesis from gel. For almost all samples, the thermal synthesis was performed

at 1420°C for 16 days, except for anorthite and $An_{60}SrF_{40}$, which were synthesized for 2 h at 1450°C and 1350°C respectively. The details on the synthesis can be obtained by the above investigations.

When the amount of the specimen was enough, X-ray powder diffraction experiments were carried out in the present investigation, in order to check the crystal symmetry (space group) and refine the unit cell parameters. The same samples were embedded in resin, polished, carbon coated and analysed by scanning electron microscopy coupled with energy dispersive spectroscopy (Figure S1).

2.1 | Powder X-ray diffraction

XRD measurements were performed with a Rigaku SmartLab XE diffractometer with θ-θ goniometer, equipped with CuKα radiation, generator working at 40 kV and 30 mA, position sensitive DteX detector 256 multistrips. Si^0 NIST 640e powder was added to the samples, to correct the refined cell parameters for any misalignment by the internal standard method. The samples were placed in flat and round sample holder and were spun during the measurement at 60 rpm. Diffraction patterns cover the range $10 < 2\theta < 100$ (step 0.01°) and were measured with a detector speed of 1°/min, resulting in a total acquisition time of 1.5 h.

The diffraction patterns were analysed and compared using Rigaku PDXL2 SOFTWARE (Figure S2) and then refined with GSASII software.[31] The employed strategy involved at first the refinement of the zero-error shift by fixing the certified Si NIST cell parameters, followed by the refinement of the feldspar cell parameters. The obtained values are reported in Table 1.

2.2 | Scanning and transmission electron microscopy

SEM and EDS analyses were performed using a JEOL JSM-IT300LV Scanning Electron Microprobe, equipped with Oxford INCA Energy 200 EDS SATW detector (WD 10 mm, KV 15). The chemical analyses were carried out, in order to verify and confirm the Ca/Sr ratio entered during the synthesis. In the EDS spectra, Kα1 line of Si (1.740 keV) and Lα1 line of Sr (1.807 keV) partially overlap, resulting in a peak broad and asymmetric. The software used for data measurement and treatment (Oxford EDS AZtec) mathematically deconvolves the contributions of the two chemical species (Figure S3). In addition, as we reported in the introduction, in the structure of feldspars, there are four tetrahedral sites T (occupied by Si and Al) and one 8–9 coordinated site M (Ca and Sr); Si and Sr, therefore, occupy different sites, and the calculation of cations per formula unit is an efficient check on the reliability of analysis. In our analyses, the calculated formula confirms the nominal Ca/Sr ratio used in the synthesis, taking into account the experimental standard variations of about 0.02 a.p.f.u. (Table 1).

The studied samples were also investigated by transmission electron microscopy, mainly by the analysis of selected area diffraction patterns. A Philips CM12 electron microscope, operating at 120 kV, side entry, was used. The samples were prepared by deposition of the crushed powder on carbon coated grids (Figure S4).

2.3 | μ-Raman spectroscopy

Raman spectra were collected on natural and synthetic crystals, using a LABRAM HRVIS–Horiba JobinYvon

TABLE 1 Unit cell parameters and calculated chemical formula for synthetic $Ca_{1-x}Sr_xAl_2Si_2O_8$ feldspars.

Sr (apfu × 100)[a]	*a* (Å)	*b* (Å)	*c* (Å)	α (°)	β (°)	γ (°)	V(Å^3)	EDS chemical formula	s.g.
0	8.175	12.873	14.170	93.11	115.89	91.28	1337.80	$Ca_{0.98}\ Si_{2.02}\ Al_{1.99}\ O_8$	$P\bar{1}$
10	8.209	12.883	14.187	93.06	115.76	91.20	1347.84	$Ca_{0.90}\ Sr_{0.09}\ Si_{1.99}\ Al_{2.02}\ O_8$	$P\bar{1}$
20	8.240	12.895	14.197	92.83	115.70	91.16	1356.49	$Ca_{0.82}\ Sr_{0.21}\ Si_{1.83}\ Al_{2.21}\ O_8$	$P\bar{1}$ diffuse
30	8.254	12.902	14.206	92.68	115.69	91.15	1360.38	$Ca_{0.73}\ Sr_{0.24}\ Si_{2.00}\ Al_{2.02}\ O_8$	$P\bar{1}$ diffuse
40	8.290	12.931	14.218	92.19	115.57	90.95	1372.97	$Ca_{0.60}\ Sr_{0.37}\ Si_{2.04}\ Al_{1.96}\ O_8$	$P\bar{1}$ diffuse
50	8.283	12.920	14.217	92.28	115.70	91.05	1368.69	$Ca_{0.49}\ Sr_{0.47}\ Si_{2.05}\ Al_{1.96}\ O_8$	$P\bar{1}$ diffuse
70	8.341	12.951	14.242	91.14	115.47	90.80	1388.33	$Ca_{0.24}\ Sr_{0.72}\ Si_{2.03}\ Al_{2.00}\ O_8$	$I\bar{1}$
75	8.345	12.952	14.248	91.31	115.53	90.85	1388.86	$Ca_{0.27}\ Sr_{0.71}\ Si_{2.05}\ Al_{1.94}\ O_8$	$I\bar{1}$
80	8.361	12.961	14.252	90.78	115.42	90.58	1394.46	$Ca_{0.22}\ Sr_{0.80}\ Si_{1.95}\ Al_{2.05}\ O_8$	$I\bar{1}$
100	8.369	12.975	14.262	90.00	115.15	90.00	1401.84	$Sr_{0.97}\ Si_{2.03}\ Al_{1.98}\ O_8$	$I2/c$

Note: The unit cell error is 0.001 for cell vectors and 0.01 for cell angles.

[a]Nominal composition.

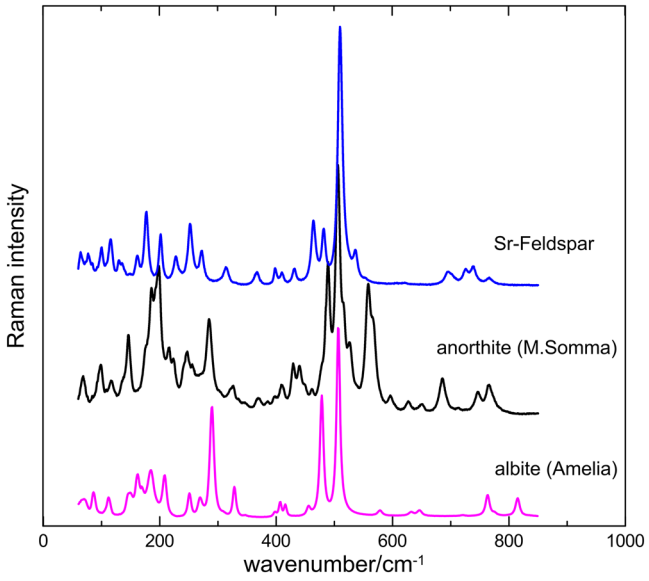

FIGURE 2 Raman spectrum of albite, anorthite and Sr-feldspar. The albite spectrum is taken from Aliatis et al.[32]

HR800 μ-Raman spectrometer (G. Scansetti Interdepartmental Center, University of Torino) equipped with a cooled CCD detector (−70°C), Nd solid state green laser (wavelength 532 nm, power 250 mW) and an 1800 grooves/mm grating, in the 60–1050 cm^{-1} range (spectral resolution of 2 cm^{-1}). Raman spectra were acquired and treated with Labspec5 software (Horiba technology). For each sample, at least five spectra were collected, to verify any possible effect of orientation, within two ranges, the first one between 60 and 850 cm^{-1} (Figures 2 and 3), and the second between 700 and 1200 cm^{-1} (Figure 4). The spectra for the two ranges were collected on the same sample, but separate sessions. The spectra were taken in casual orientation; for a given composition they are quite similar, likely as the examined grains are a mixture of crystals with different orientation, mostly due to twinning. Peak positions were obtained by fitting with a Gaussian function, in view of the highly disordered nature of intermediate compositions, as discussed in the following; for a given composition, the peak positions are within resolution error (Figure S5).

3 | RESULTS AND DISCUSSION

3.1 | Phase transitions and Raman spectra in $Ca_xSr_{1-x}Al_2Si_2O_8$ feldspars

The highest symmetry topologic structure of feldspars is the *C*2/m structure of the disordered sanidine ($KAlSi_3O_8$). In *C*2/*m* sanidine, seven independent atoms form the asymmetric unit, and the repetition along the c axis is about 7 Å. The same structure occurs in monoclinic feldspars when they have a fully disordered distribution of Al and Si; it was found for instance in fully disordered lead and Sr-feldspars.[33,34] Group theory predicts for the structure of disordered *C*2/m feldspar 20 A_g + 19 B_g Raman active modes.

Distortion of the *C*2/m configuration leads to the $C\bar{1}$ triclinic structure in albite, in which 39 A_g Raman active peaks are predicted,[32] as a consequence of the increased number of non-equivalent atoms. Al and Si in albite are present in four non-equivalent sites; in fully disordered albite, they are occupied by 0.25 Al atom each one, whereas in fully ordered albite, Al is confined in one of the four sites. In plagioclase with Al:Si approaching 1:1, and ordered Al-Si configuration, the structure becomes $I\bar{1}$, with doubled cell along the c axis. In the $I\bar{1}$ structure, group theory predicts 78 A_g Raman active modes. Further distortion occurs at compositions close to anorthite, with $P\bar{1}$ structure where we have 52 independent atoms in the 14 Å cell and 156 A_g Raman active modes. In feldspars with Al/Si 1:1, disordered Al/Si configurations are energetically unfavourable, for that Al-O-Al would inevitably form in a disordered configuration, violating the so called 'Al-avoidance rule'.[35] Therefore, natural anorthite is almost completely ordered.[36] However, in Pb and Sr feldspars, the rule is less strict, and samples with disordered Al/Si configurations can be easily synthesized.[33,34,37] Further complexities arise for incommensurate modulations, and non-periodic mottled $P\bar{1}$ structures. Incommensurate modulations were found in plagioclase with intermediate Na/Ca content and in anorthite at the very beginning of the devitrification from amorphous[38]; non-periodic mottled textured were found in synthetic anorthite and Ca-richer $Ca_{1-x}Sr_xAl_2Si_2O_8$ feldspars.[5,10,39] The mottled structures are related to the strain induced by local $P\bar{1}$ configurations, in a sample compositionally homogeneous. Their structure was described by TEM analysis.[39]

Monoclinic feldspars with Al/Si 1:1 with ordered Al:Si configuration show a *I*2/*c* structure, of which the $I\bar{1}$ is a distorted triclinic derivative (Figure 1). In the *I*2/*c* structure, we have 39 A_g and 39 B_g Raman active modes. The *C*2/m structure is observed in monoclinic Sr-feldspar after quenching from gel or glass, when it retains a metastable highly disordered Al/Si configuration; in anorthite instead, Al-Si order is found even in the synthetic samples after extremely fast crystallization from melt.[38] In $Ca_{1-x}Sr_xAl_2Si_2O_8$ feldspars, the symmetry changes with composition, from $P\bar{1}$ to $I\bar{1}$ and *I*2/*c* as Sr increases. The critical composition at which the transition from the $P\bar{1}$ to $I\bar{1}$ structure occurs is ill defined, whereas Landau theory-based analysis of the spontaneous strain pinpoints the onset of the monoclinic structure between x = 0.6 and 0.91, in dependence of the annealing time and

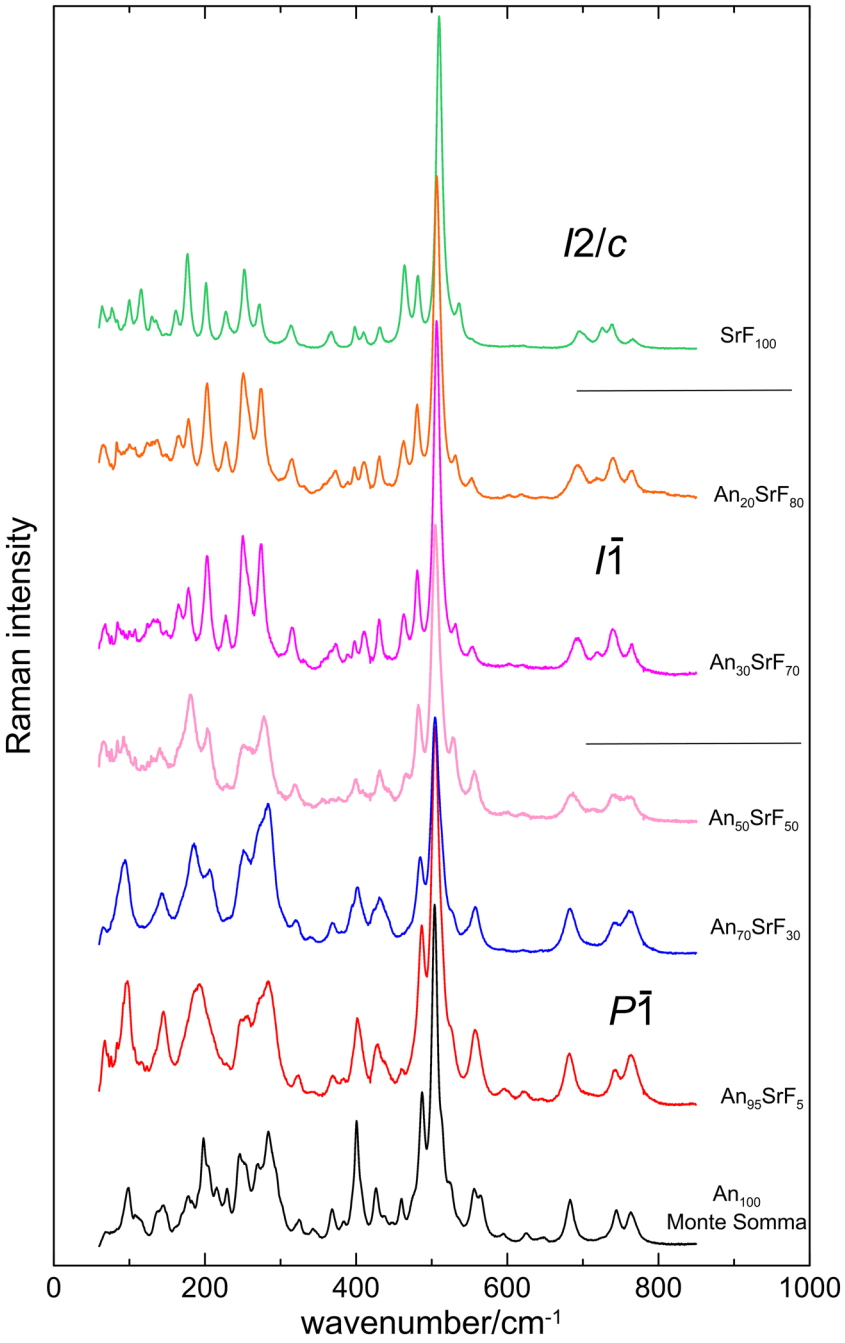

FIGURE 3 Lower wavenumber (60–850 cm^{-1}) Raman spectra of $Ca_{1-x}Sr_xAl_2Si_2O_8$ feldspars. Only a selection of the collected spectra is shown. The lines on the right divide the $P\bar{1}$, $I\bar{1}$ and $I2/c$ spectra from bottom to top, here and in Figure 4. Only a selection of the spectra, without a specific orientation, is reported here and in Figure 4.

temperature before the high temperature measurement, in turn related to Al-Si order.[8,9]

The spontaneous strain for the $P\bar{1}$ to $I\bar{1}$ transition is rather small,[40,41] but the onset of the transition can be constrained by the analysis of the selected area TEM diffraction patterns.[5] The $P\bar{1}$ structure shows four types of reflections, named: *a*, with indexes h + k even, l even; *b* h + k odd, l odd; *c* h + k even, l odd and *d* h + k odd, l even. In the $I\bar{1}$ and $I2/c$ structures the *c*- and *d*-type reflections are absent whereas in $C\bar{1}$ and $C2/m$ also the *b* type is absent. In natural anorthite, and the Ca richer feldspars synthetized by longer hydrothermal annealing all the above reflections are present. In synthetic $P\bar{1}$ feldspars, the *d* type reflections are absent, and only more or less diffuse and elongated *c* type reflections are present. In feldspars with higher Sr content only *a*- and *b*-type reflections are present indicating a body-centred structure. Analysis of the SAED patterns showed that sharp *c* and *d* reflections were found only between anorthite and $An_{90}SrF_{10}$ and that the elongated *c*-type reflections disappear at about $An_{50}SrF_{50}$, although the exact point for the transition is ill defined (Figure 5).[5]

The above description accounts for natural feldspars and their derivatives. Within the composition of 1:1 Al/Si Ca, Ba and Pb feldspars hexagonal, zeolite-like and other derivatives exist, which will not be accounted here.[42–44]

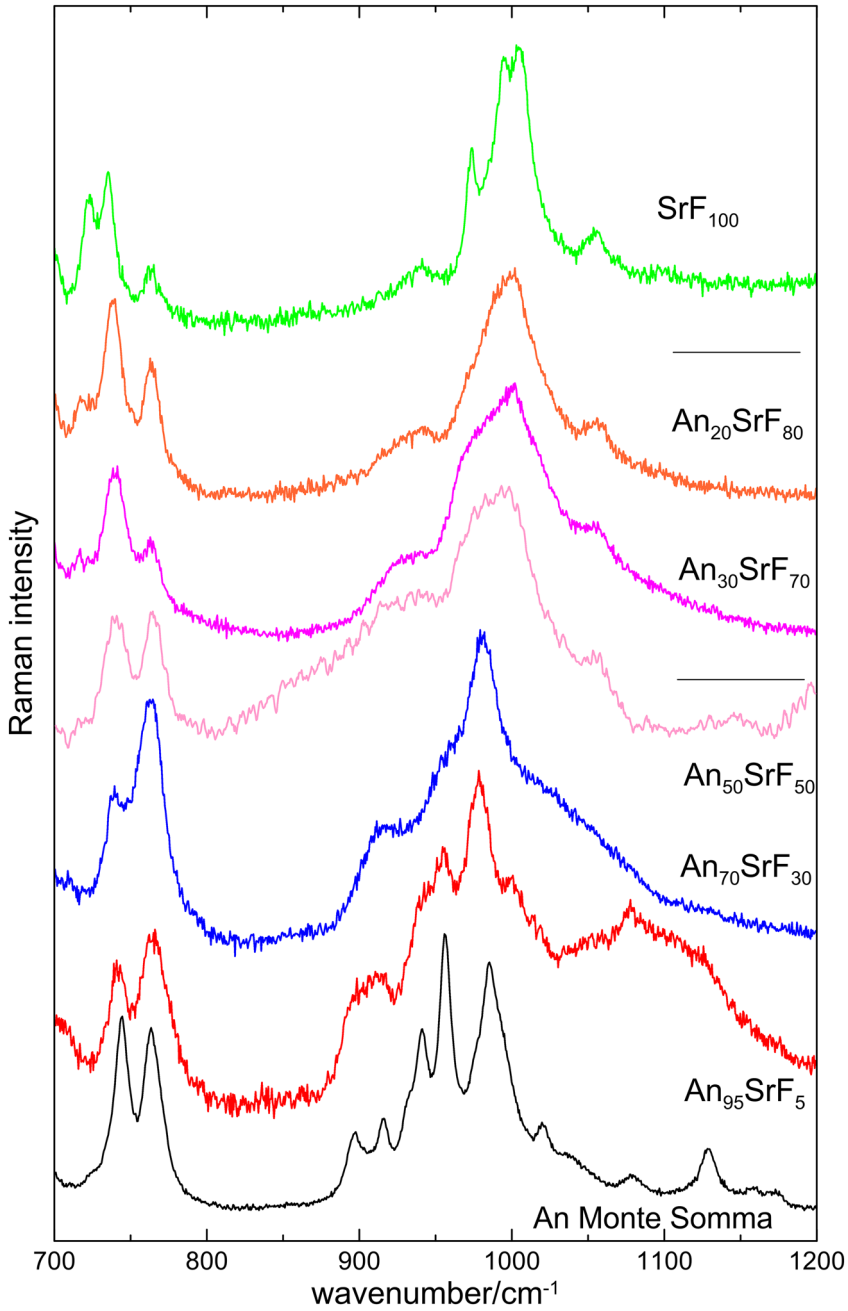

FIGURE 4 Higher wavenumber (700–1200 cm^{-1}) Raman spectra for $Ca_{1-x}Sr_xAl_2Si_2O_8$ feldspars.

3.2 | Raman spectra of Al-Si 1:1 feldspars

A problem in the analysis and interpretation of the Raman spectra in the Ca-Sr feldspars is the ubiquitous occurrence of twinning according to the Carlsbad and Albite laws. Carlsbad twins are originated by 180° rotation of the individuals along [001] with (010) composition plane. Carlsbad twins are present throughout the series in monoclinic and triclinic Ca-Sr feldspars. In synthetic Ca-Sr feldspars, Carlsbad twins occur polysynthetically with repetition of a few unit cells. Carlsbad twins are more frequent as Sr content increases, due to better fit at the interface between rotated twins.[10] A second kind of twinning is Albite twinning. Albite twinning is due to a mirror plane on (010), with twin axis [010] and composition plane (010). As the mirror plane exists in monoclinic, but not in triclinic lattice, Albite twins are present, together with Carlsbad twins, in triclinic Ca-Sr feldspars only. Respect to natural feldspars, where such twins are visible at the optical microscope scale, here, they are sized just a few unit cells,[5,10,11] and may be detected only by transmission electron microscope. Therefore, for any triclinic grain we have four coexisting orientations, each of them in a non-predictable contribution. This obviously affects the Raman spectra when trying to perform an observation according to a given orientation: even for the same orientation we may observe different spectra according to the different proportion of the twin orientations.

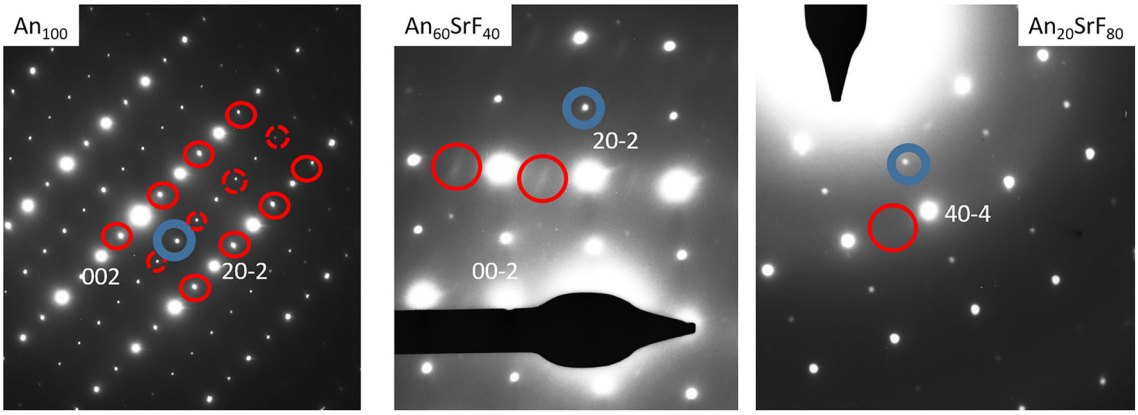

FIGURE 5 Selected area diffraction patterns for Ca-Sr feldspars. The sample composition is given in the inset. In the An_{100}, c-type reflections are red circled, d-type reflections are red and dashed, and a single b-type reflection is bold blue circled. Diffuse c-type reflections are shown for $An_{60}SrF_{40}$ (indexed 201 and 20-1), compared with the sharp b-type (blue circled, indexed 30-3); in $An_{20}SrF_{80}$, no reflection is present where c-type reflections should be present, whereas b-type reflections are still sharp (blue, 30-3).

In this work, the strategy was then to collect a number of spectra with different orientation and to discuss in terms of peak positions rather than peak intensities, which are biased by the non-predictable ratio between the different twins. The following description will therefore rely on peak positions only.

An assignment of Raman peaks and description of their mode vibrations in feldspars were done in $C\bar{1}$ albite by lattice dynamics and quantum mechanical calculations.[32,45,46] This makes a basis for the interpretation of the Raman spectra in Ca-Sr feldspars, although in $P\bar{1}$, $I\bar{1}$ and $I2/c$ feldspars with Al/Si 1:1, a number of peaks not found in albite are present. Moreover, the phase transitions add further intricacies, changing peak position and intensity of the peaks present in albite. Tables 2 and 3 summarize the positions of the peaks detected in natural anorthite and synthetic Ca-Sr feldspars.

In Figure 2, the Raman spectra of $C\bar{1}$ albite, $P\bar{1}$ anorthite and $I2/c$ Sr-Feldspar are shown. The description of the peaks will take advantage of the peak assignment done for albite.[32] The albite structure has a topological framework that is almost the same as other feldspars in different space groups. The different space groups arise structurally for symmetry breaking distortions and intersite order–disorder within a structure whose building blocks are unchanged. The following description is the results of a number observations on several grains for each composition, assumingly with different orientation. The spectra reported in Figures 3 and 4 are sample spectra to show the general variability and highlight the grouping discussed in the following paragraph.

A first group of cage-shear modes is present below 200 cm^{-1}. They are related to translations of the non-tetrahedral cations, together with rigid rotation of the tetrahedra. These modes are the only ones where the non-tetrahedral cation is involved directly. The first three modes in albite are at 66, 73 and 92 cm^{-1}: in anorthite we have two peaks at 67 and 92. The peak at 92 cm^{-1} is found in natural and synthetic anorthite; as Sr increases its intensity decreases. In Sr-feldspar four well resolved peaks at 65, 77, 100 and 115 cm^{-1} are present (Figure 3).

At higher wavenumbers, in albite we find a peak at 148 cm^{-1}; in anorthite, it becomes a doublet, almost at the same position. It becomes broader in intermediate Ca-Sr compositions. We observe a doublet in feldspars with Sr > 0.5 apfu at 125–130 cm^{-1} and a peak at 115 cm^{-1} in monoclinic Sr-feldspar (Figures 3 and 6).

In natural anorthite, seven peaks were detected between 175 and 225 cm^{-1}, at 175, 187, 200, 206, 215 and 222 cm^{-1}, of which the peaks at 187 and 200 cm^{-1} form a doublet (Table 2). In synthetic anorthite and in intermediate Sr-feldspars, the two peaks of the doublet are barely resolved. At Sr > 0.5 apfu a new peak appears at 165 cm^{-1}. In Sr feldspar, we see three sharp peaks at 162, 177 and 201 cm^{-1}. The position of the peak at 187 cm^{-1} changes significantly with composition (Figure 7), providing a marker for the $P\bar{1}$ to $I\bar{1}$ transition.

The peaks between 200 and 400 cm^{-1} were assigned in albite to bending motion and deformation of tetrahedral rings. In albite, we have six peaks, calculated and observed, at 251, 269, 290, 308, 328 and 353 cm^{-1}. A number of superimposed peaks was found for anorthite in this region, 11 of which could be identified, at 222, 239, 246, 255, 270, 284, 320, 326, 334, 368 and 384 cm^{-1}. In the synthetic anorthite, a broad band between 230 and 300 cm^{-1} is present, in which only the peak at 290 cm^{-1} could be resolved. Between $An_{30}SrF_{30}$ and Sr-feldspar, two peaks resolve the large band, at 252 and 275 cm^{-1}, and a new peak is observed at 226 cm^{-1}, hardly detectable in Sr poorer feldspars for

TABLE 2 Raman peak positions (cm^{-1}) in natural and synthetic anorthite.

1	Natural	Not measured				135	144		166			197	205			246		268	283	291			333	342	368	383		400			427	437
2	Natural	70	91	98	111	116	134	145	159	174	184	190	197	216	221	229	244	254	265	283	291	300	318	325	339	367	383	393	400	405	410	427	439
3	Natural	68	93	98	108	117	137	146		175	186		197	215	223	239	246	255	270	284			321	326	334	368	384		397	409		428	439
4	Synthetic	67		96				144			188		206					253	272	288				323	341	369			403			428	440
5	Synthetic	63	88				139				182		200					253	273	281			316			369			400			427	
1	Natural	459	476	488		503	513	522		532			565			682			761	764				914	929		954	972	985	not measured				
2	Natural	459	474	487		504	514	524		537	555	565	601		639	684	702	744	762		825	847		914	931	941	954		988	1006	1019		1082	
3	Natural	461	476	488		505	515	524			556	565			625	684	711	744	764				896	914	939		956		985	1007	1019	1035	1078	1128
4	Synthetic		486		506			524			558		597		622	682		740	765					910			958	977	997				1066	1126
5	Synthetic		484		503						553		590		620	681		741	756					908			949	974	998		1044	1072	1124

Note: Data from 1. Daniel et al.,[47] Val di Fassa (named Val Pasmeda) An_{100} anorthite; 2: Bersani et al.,[46] Val di Fassa (named Val Pasmeda) An_{100} anorthite; 3: this work: natural, Vesuvio (also named Monte Somma; $Ca_{0.95}Na_{0.03}Al_{1.97}Si_{2.04}O_8$); 4: An_{100}, this work, synthesized for 2 h at 1450°C from gel; 5: Matson et al.,[48] synthesized from glass after 24 h annealing at 1000°C.

any orientation,. In this group the peak at 284 cm^{-1} in anorthite shows the greatest change, down to 270 cm^{-1} in Sr-feldspar. The triplet at 320 cm^{-1} in anorthite could not be further resolved, and a single peak at 320 cm^{-1} is present. The peak at 320 cm^{-1} shifts at 312 cm^{-1} in Sr-feldspar.

The peaks between 400 and 560 cm^{-1} were related in albite to ring breathing motion. The peaks in this range are the most intense in feldspars. Twelve independent and overlapping peaks were measured in natural anorthite, at 397, 409, 428, 439, 461, 476, 488, 505, 515, 524, 556 and 565 cm^{-1}, which reduce to seven in Sr-feldspar. In albite, in the same range we find eight peaks, at 398, 410, 419, 466, 485, 492, 513 and 579 cm^{-1}. With increasing Sr the two peaks between 397 and 409 merge in a single peak at 403 cm^{-1}; the position of this peak decreases to 398 cm^{-1} in monoclinic Sr-feldspar; a new peak appears at 410 cm^{-1} in feldspars with Sr > 0.7 apfu. The doublet at 428 and 439 cm^{-1} in anorthite is broader in intermediate solid solutions, and for $I\bar{1}$ feldspars, the peak at 439 cm^{-1} is hardly detected; in Sr-feldspar, only a peak at 430 cm^{-1} occurs. The peak at 461 cm^{-1} is barely visible between An_{100} and $An_{90}SrF_{10}$ below the stronger peak at 485 cm^{-1} in intermediate compositions; in compositions Sr-richer than $An_{35}SrF_{65}$, it becomes sharper. The peak at 476 cm^{-1} in natural anorthite is a shoulder of the peak at 488 cm^{-1}, and it was not resolved in other feldspars. The peak at 505 cm^{-1} is the strongest in feldspars; its wavenumber increases by 3 cm^{-1} between anorthite and Sr-feldspar. The difference between the peaks at 487 and 505 cm^{-1} is more sensitive to compositional changes: it increases by 9 cm^{-1} between anorthite and Sr-feldspar. The peaks at 515 and 524 cm^{-1} are resolved only in natural anorthite. They merge becoming a shoulder at 520 cm^{-1} of the peak at 505 cm^{-1}. Such shoulder is hardly resolved in more anorthitic samples, but becomes better shaped in Sr-richer ones. The doublet at 556 and 565 cm^{-1} in natural anorthite is not resolved in other feldspars; in plagioclase the doublet was resolved only in anorthite.[46]

The peaks from 600 to 900 cm^{-1} were assigned to tetrahedral framework deformation modes in albite. In this range, seven peaks could be identified in natural anorthite, respectively at 595, 625, 648, 685, 712, 745 and 763 cm^{-1}. The peaks at 595, 625 and 648 cm^{-1} are rather weak; they are not visible in monoclinic Sr-feldspar, being present only in triclinic feldspars. Most intense in the range are a single peak at 685 cm^{-1} and a doublet at 745–763 cm^{-1}.A peak at 720 cm^{-1}, which is barely detected between anorthite and $An_{30}SrF_{70}$, is clearly observed between $An_{30}SrF_{70}$ and $An_{20}SrF_{80}$, and has the same intensity of the peak at 690 cm^{-1} in SrF. The peak at 685 cm^{-1} in anorthite increases its wavenumber with

TABLE 3 Raman wavenumber (cm^{-1}) in $Ca_{1-x}Sr_xAl_2Si_2O_8$ feldspars.

An100	67			96			144		188	206		253	272	288	323	341	369	403	
$An_{95}SrF_5$	66			97			144		188	207		250	269	285	323		369	403	
$An_{90}SrF_{10}$	66			96			144		186	209		252	269	286	323		377	403	
$An_{80}SrF_{20}$	66			94			144		187	207		252		285	323		371	402	
$An_{70}SrF_{30}$	65			93			142		186	207		252	269	283	321	340	369	402	
$An_{60}SrF_{40}$	67		85	92		130	144		183	201		257		281				402	
$An_{50}SrF_{50}$	66			93		129	141		181	204		250		278	320			401	
$An_{40}SrF_{60}$	67		84	99		124		166	178	203	227	253		276	316			398	
$An_{35}SrF_{65}$	67		84	100		126		165	179	202	227	252		275	315		365	398	412
$An_{30}SrF_{70}$	67		85	99		129		165	179	203	226	252		275	316		369	398	410
$An_{25}SrF_{75}$	68		84	101		133		163	178	202	227	252		274	315		371	397	410
$An_{20}SrF_{80}$	66		84	98	119	132		165	178	203	227	253		274	315		370	398	410
SrF_{100}	65	77	84	100	115	129	135	162	177	201	227	252		271	313		365	398	409

TABLE 3 (Continued)

An100	428	440		486	506	524	558	597	622	682		740	765	910		958	977	997	1066
$An_{95}SrF_5$	427	438		487	505	521	559	598	622	683		741	764	911		954	978	994	1066
$An_{90}SrF_{10}$	430	441		486	505	524	559	595	622	683		740	764	911		957	977		1069
$An_{80}SrF_{20}$	429	441		486	505	524	558		621	683		739	764	912		957	978		1059
$An_{70}SrF_{30}$	433	441		485	505	525	558	593	621	683		739	762	914		957	979		1047
$An_{60}SrF_{40}$	432	439	455	485	506	523	558	599	623	686		741	766	912		954	984		1046
$An_{50}SrF_{50}$	431	443	466	483	505	526	556		621	686	715	740	762	912			982		
$An_{40}SrF_{60}$	430		463	480	507	527	554	599		690		739	762	916			985		
$An_{35}SrF_{65}$	431		464	481	506	527	556			692	720	741	764		943		999		1054
$An_{30}SrF_{70}$	430		465	481	506	530	554	601	618	691	718	740	764		942		995		1058
$An_{25}SrF_{75}$	431		463	481	506	529	553	600	619	691	718	740	763		941		995		1057
$An_{20}SrF_{80}$	431		462	481	507	531	554			693	720	739	763		941		996		1056
SrF_{100}	430		463	480	509	533				694	723	736	763		942	973	996	1004	1056

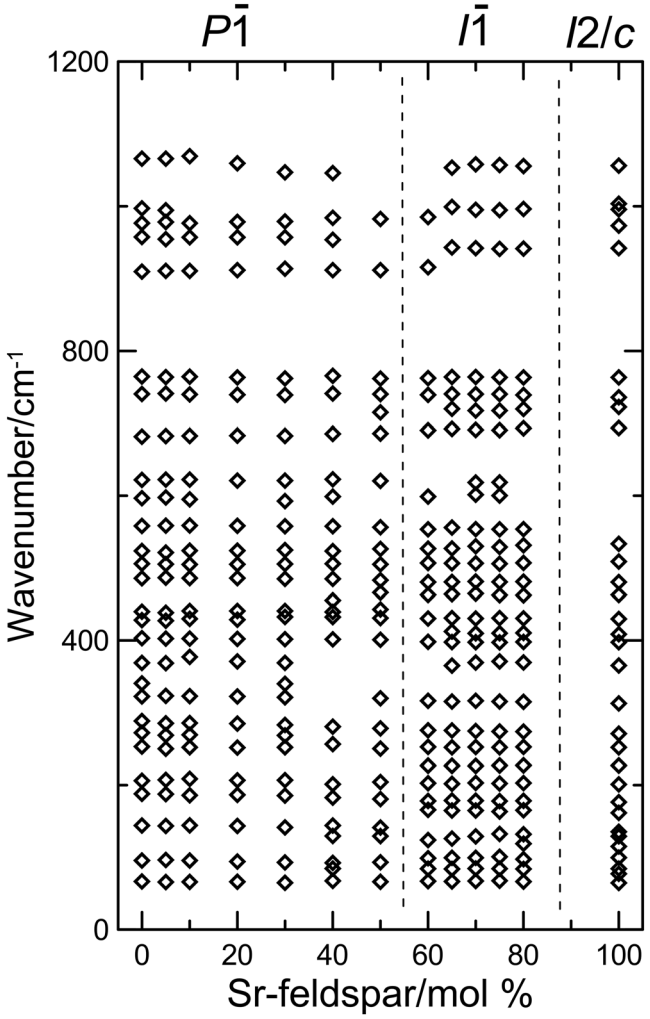

FIGURE 6 Raman peak positions and phase transitions for $Ca_{1-x}Sr_xAl_2Si_2O_8$ feldspars. The figure is meant to show the positions of the measured peaks without ascribing them to a specific mode. The error is within the size of the symbol.

Sr (Figures 3 and 7) up to 690 cm^{-1} in Sr-feldspar, whereas the position of the two peaks at 740 and 764 cm^{-1} do not change significantly with composition.

The peaks from 900 to 1200 cm^{-1} were ascribed in albite to intra-tetrahedral stretching modes. In natural anorthite, we have a number of large overlapping peaks at 896, 914, 939, 956, 985, 1007, 1019, 1035, 1078 and 1128 cm^{-1}. In other compositions, we find a large band, with a maximum between 970 and 1020 cm^{-1}, and poorly resolved sidebands (Figure 4). Between $An_{50}SrF_{50}$ and $An_{30}SrF_{70}$, the maximum of the broad band shifts from 982 to 995 cm^{-1}. The peaks at 1078 and 1128 cm^{-1} are found only in anorthite and $An_{95}SrF_5$. In Sr feldspar, only five peaks at 938, 973, 995, 1005 and 1054 cm^{-1} occur, of which the strongest ones are in the triplet between 973 and 1005 cm^{-1}.

3.3 | Raman peaks and short-range symmetry

From the observation of the Figures 3 and 4, we can group the Raman spectra of the Ca-Sr feldspars in four types, with changing composition from anorthite to Sr-feldspar. The grouping will be here discussed in relation to previous observations on the symmetry and microstructures as determined by TEM and XRD.[5,10,11]

First, natural anorthite shows a large number of relatively sharp peaks, often split like that at 560 cm^{-1}. In selected area diffraction patterns, *c*-type reflections of pure anorthite are round and sharp, and the symmetry is $P\bar{1}$. By heating at 516 K or compressing at 2.6 GPa, the structure shifts to the $I\bar{1}$ structure.[47,49,50]

Synthetic anorthite and feldspars up to $An_{60}Sr_{40}$ make a second group: Their peaks are similar in shape and position to natural anorthite, but broadened and less resolved. This indicates a persistence of the $P\bar{1}$ symmetry of anorthite, as previously suggested by TEM. In the Ca-richer feldspars, synthetic anorthite and $An_{95}SrF_5$, TEM observation showed that *c*-type reflections are sharp, but elongated. High temperature powder diffraction showed a small spontaneous strain for the transition from the high temperature $I\bar{1}$ to the $P\bar{1}$ structure between 100 and 200°C.[6] What is observed for Ca-richer feldspars by TEM is similar to the findings for anorthite with little solution of the albite molecule. For instance, natural Na-richer anorthite, like the Mijake ($An_{96}Ab_4$), shows broader Raman peaks and a single peak at 560 cm^{-1}.[46] In Mijake anorthite, the *c*-type reflections are elongated and become diffuse in samples with higher sodium. The Na-richer anorthites were reported as transitional, although the average primitive crystal structure is similar to pure anorthite: he difference is not in the average structure, but in the size and shape of the primitive antiphase domains.[51,52] In transitional anorthite, the primitive antiphase domains are smaller than 100–200 Å, and elongated, whereas in natural pure anorthite, they are sized few thousand Å.[38] Also, transitional anorthites undergo a transition to the $I\bar{1}$ structure at higher temperature, but the transition occurs at lower temperature and pressure and shows a second order behaviour.[36,41]

In Ca-poorer feldspars of the second group, between $An_{90}Srf_{10}$ and $An_{60}SrF_{40}$, no spontaneous strain is found, but SAED patterns show faint *c*-type reflections, visible only when enhanced by the longest exposures, indicating poor long-range coherency (Figure 5). A $P\bar{1}$ symmetry for these compositions was also indicated by the analysis of the mechano-luminescence behaviour for intermediate feldspars with $(Ca_xSr_{1-x})Al_2Si_2O_8$ compositions.[28] The positions for several well-detectable Raman peaks change

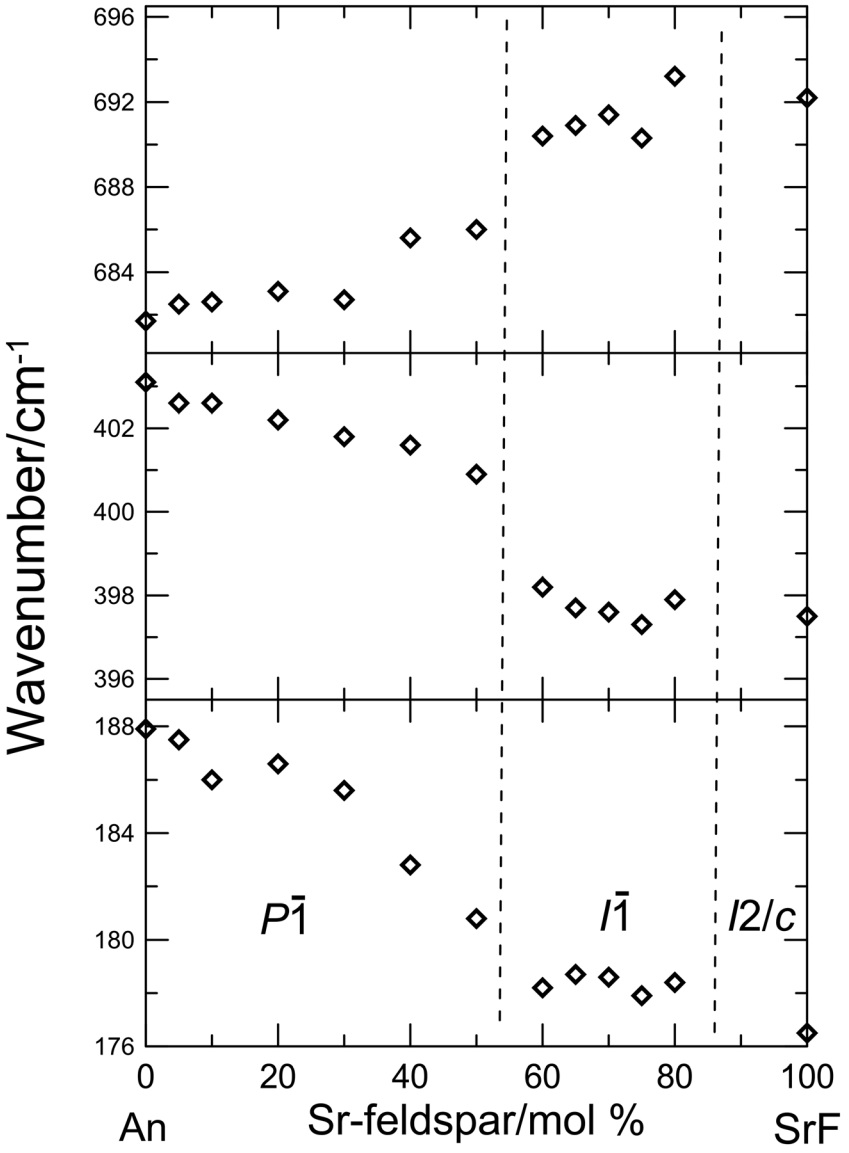

FIGURE 7 Peak shift and phase transitions in $Ca_{1-x}Sr_xAl_2Si_2O_8$ feldspars.

little within the compositional range of the second group, but have a sudden shift at $An_{50}SrF_{50}$. This observation together with the SAED and mechanoluminescence evidence points out that all the feldspars of the second group share a $P\bar{1}$ symmetry.

The appearance of the Raman spectra, taken in different orientations for $An_{50}SrF_{50}$, is intermediate between the second group and the third group (Figures 3 and 4). The $An_{50}SrF_{50}$ spectra show already several features present in the $I\bar{1}$ Sr richer samples: The shoulder at 520 cm^{-1} becomes a more distinct peak, and a weak peak at 712 cm^{-1} appears. However, peak positions intermediate between $P\bar{1}$ and $I\bar{1}$ are found (Figure 7), and the doublet at 430 cm^{-1}, which becomes a singlet in $I\bar{1}$ feldspars, has a shoulder, like in $P\bar{1}$. Also, the band at higher wavenumber has a maximum at 990 cm^{-1}, like in $P\bar{1}$ feldspars. In the same sample, overexposed SAED patterns revealed diffuse *c*-type reflections. The indication is that at a short-range scale, $P\bar{1}$ and $I\bar{1}$ configurations coexist, possibly with primitive clusters.

A third group, between $An_{40}SrF_{60}$ and $An_{20}SrF_{80}$, shows better resolved peaks, a different maximum in the disordered 950–1050 cm^{-1} band and features intermediate between the first two groups and Sr-Feldspar. TEM data did not show *c*-type reflections, not even in the longest exposures. For the $An_{20}SrF_{80}$, also single crystal diffraction confirmed that the structure is $I\bar{1}$.[12]

The fourth group is Sr-feldspar, which has unique features, like the four resolved peaks between 60 and 120 cm^{-1} and three well-resolved peaks instead of the 950–1050 cm^{-1} band. TEM and single crystal X-ray diffraction show that Sr-feldspar has *I*2/c structure.[10,33,53]

3.4 | Spontaneous strain, long range symmetry, Al-Si order and phase transitions

The exchange of Sr for Ca increases unit cell volume and promotes two transitions: one between $P\bar{1}$ and $I\bar{1}$ and the other between $I\bar{1}$ and $I2/c$. The second one is well constrained by the unit cell parameters, as the α and γ unit cell angles change by 3 and 1° between triclinic anorthite and monoclinic Sr-Feldspar. It is a ferroelastic transition, due to a distortion of the framework structure of feldspars in presence of a larger cation like Sr.[54] The monoclinic structure is found also in other feldspars where Ca is exchanged for a larger cation, like Pb or Ba. Such distortion may occur also in fully Al/Si ordered feldspars. Previous solid-state NMR investigation on ^{29}Si and ^{27}Al showed that all Ca and Sr feldspars are quite ordered, although with some difference in the degree of Al-Si order with composition[55]; long range ordering can be achieved by annealing a metastable sample,[33] indicating that at equilibrium Sr-feldspar in most conditions shows an Al-Si ordered configuration. Only close to the subsolidus, above 1560°C, deviations from equilibrium ordered configuration are observed in Sr-feldspar.[56]

Landau theory identifies for the triclinic to monoclinic transition an order parameter (Q_D); it was shown that Q_D is proportional to the spontaneous strain for the transition (e_{ss}), in turn proportional to cosα*.[57] In a second order transition Q_D^2 is proportional to the composition (X), and a coupling with composition of the type $X \propto Q_D^2 \propto \cos^2\alpha^*$ is expected.[57]

The linear trend shown in figure between composition and $\cos^2\alpha^*$ indicates that a second order behaviour is indeed present (Figure 8). The transition between triclinic and monoclinic for this work samples occurs at $X_{Sr} = 0.86(3)$. The critical composition for the transition is Sr-richer than in Zhang et al. (2010)[27] and Feng et al. (2020),[29] respectively $X_{Sr} = 0.80$ and 0.75 and lower from that determined by McGuinn and Redfern (1994) ($X_{Sr} = 0.91$).[52] This is likely due to different annealing conditions, inducing different degree of Al-Si order. Tribaudino et al. (1993)[9] showed that the critical composition and the order of the transition change to lower Sr content and first order in samples that underwent shorter annealing from gel. Moreover, McGuinn and Redfern (1994)[54] showed that a coupling with Al-Si order or some other unknown parameter affects the ferroelastic transition. The present data, which were not aimed to a discussion of the spontaneous strain, do not provide evidence of coupling or deviations from a second order behaviour, if not for the deviation from the $X_{Sr} \propto \cos^2\alpha^*$ linear trend in the pure anorthite.

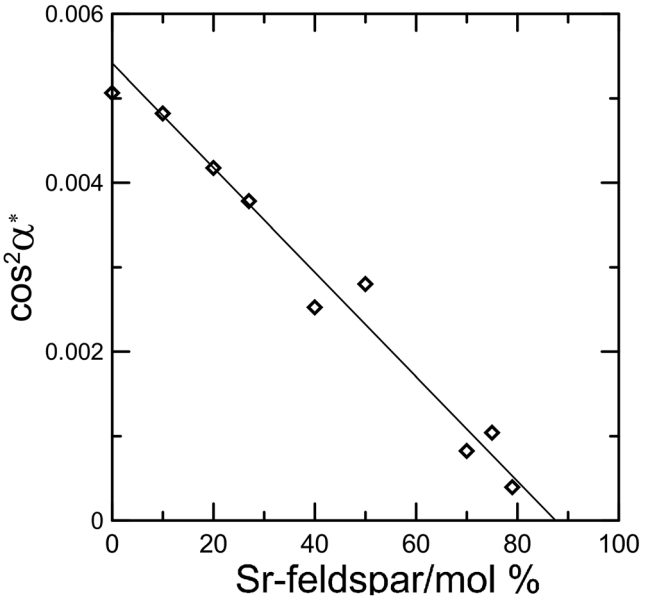

FIGURE 8 $\cos^2\alpha^*$ versus composition. The linear fit was done without the datum for pure anorthite. The error in composition and unit cell is within the size of the symbol.

3.5 | Defect structure, modulations and mechanoluminescence

In Ca- and Sr-feldspars, the ML intensity increases from anorthite to $An_{60}SrF_{40}$, and then it decreases until disappearing at $An_{20}SrF_{80}$.[29] Such disappearance was related to the "morphotropic phase transition in $Ca_{1-x}Sr_xAl_2Si_2O_8$ ($0 \le x \le 1$) ... at x = 0.86, around which the ML intensity drops to zero in the Eu^{2+} doped phosphors."[26] In a more recent paper, Feng et al.[29] showed that both phase transitions $P\bar{1}$ to $I\bar{1}$ and $I\bar{1}$ to $I2/c$ affect the mechano-luminescence. Moreover, in the composition where the maximum mechano-luminescence effect was observed, we are close to the transition between the $P\bar{1}$ and $I\bar{1}$ structure. This suggests that microstructures related to the phase transitions provide symmetry related traps for the mechano-luminecent atoms. Here we propose a mechanism to account for the mechanoluminescence effects, by considering the short-range symmetry shown by Raman and previous observations on microstructures by TEM. The present model is a suggestion to be confirmed by further investigation.

Microstructures provide traps, i.e. sites where luminescent atoms may be pinned, especially on their boundaries, which may affect the optical properties of the solid compound. The traps can host luminescent dopants, which will be activated by stress and induce mechanoluminescence (ML). Ca-Sr feldspars show a variety of defect structures, with boundaries where the luminescence carrier can be released by external stress.[5,10]

Several microstructures provide traps that could host luminescent atoms in Ca-Sr feldspars. They are *c* and *b*-type antiphase boundaries, albite and Carlsbad twin interfaces and mottled non-periodic structures.

c-type antiphase boundaries are shown by TEM, in a dark field image on *c*-type diffractions. They divide domains ordered and anti-ordered as concerns the framework deformation in the $P\bar{1}$ structure.[49] They occur in natural anorthite, but in the synthetic one, in $Ca_{1-x}Sr_xAl_2Si_2O_8$ feldspars and at higher temperature, the boundaries are less defined, and a modulated structure occurs instead.[39]

b-type antiphase boundaries are again imaged by dark field electron microscopy, but on *b*-type reflections. The boundaries divide areas within a homogeneous Al-Si ordered configuration, i.e. the domains. Disordered Al-Si feldspars, obtained after very short annealing from gel or glass, show a *C*-1 structure (or *C*2/m for fully disordered pure Sr-feldspar) and no *b*-type domains; ordering of Al-Si cations occurs with the growth of *b*-type domains. The size of the domains increases with annealing, and Al-Si order increases. The *b*-type domains are not mobile, they are present for any composition in ordered Ca-Sr feldspars, and they do not disappear in monoclinic Sr-richer compositions, so they do not explain the disappearance of the mechano-luminescence in monoclinic feldspars.

Carlsbad twins in synthetic Ca-Sr feldspars occur polysynthetically with repetition of a few unit cells.[10] They are mostly found in samples after short annealing, and more in Sr-richer compositions. Their boundaries may be a trap for the luminescent cation, but they are present also in $I\bar{1}$ and monoclinic feldspars, as the rotation on the [001] is a symmetry element missing in the group symmetries of *I*2/*c*.[58] Moreover, a higher wavenumber was observed in Sr-richer feldspars.[10] If the mechano-luminescence was due to atoms trapped in the Carlsbad twin boundaries, we could expect to be even higher in Sr-richer feldspars.

Albite twins occur only in triclinic feldspars, either *C*-1, $I\bar{1}$ or $P\bar{1}$; at the composition plane, specific atoms could be pinned. Albite twins showed mobile boundaries with temperature[10] and are present also in $I\bar{1}$ Sr-rich feldspars. The difference in threshold and peak luminescence between $P\bar{1}$ and $I\bar{1}$ feldspars, observed by Feng et al.[29] could be explained by a different and less efficient detrapping in $I\bar{1}$ feldspars, related only to Eu^{2+} trapped in Albite twin boundaries.

Mottled non-periodic structures occur in intermediate compositions. The $P\bar{1}$ structure in natural anorthite occurs with large and homogeneous domains of primitive symmetry, in antiphase between each other; such domains at higher temperature, close to the temperature for the HT $P\bar{1}$–$I\bar{1}$ transition, transform to smaller mobile domains, and the c-reflections become diffuse.[49] The same was observed in Ca-richer $Ca_{1-x}Sr_xAl_2Si_2O_8$ feldspars.[5,10] Raman observations on the peak positions and overall spectral appearance suggest that for intermediate $Ca_{1-x}Sr_xAl_2Si_2O_8$ feldspars the structure is locally $P\bar{1}$, whereas at long-range order, the only evidence for a $P\bar{1}$ structure comes from very diffuse *c*-type reflections in SAED patterns. In anorthite, the annealing of a natural sample promoted the formation of smaller domains: HRTEM investigation showed that they are actually non-periodic modulations of the primitive structure.[39] Annealing and Sr exchange for Ca were found to reduce the amplitude of the modulations[5] (Figure 9). We may assume that the luminescent carrier, namely Eu^{2+}, may be present in a local $P\bar{1}$ configuration in such modulations. At these conditions, the structure is energetically very close to a $I\bar{1}$ configuration, which can be triggered by compression: It was found that the *P-I* transition can be induced by compression in anorthite.[36] The suggestion is that when the emitting atoms are trapped in modulated structures, mechanical stress could promote the transition at the local scale of the luminescent atom to a $I\bar{1}$ structure, with relaxation of the strain, detrapping and emission.

This leaves with two possible microstructures, to explain the different mechano-luminescence efficiency along the series: (1) mobilization by compression of albite twins, but not of Carlsbad ones, which could explain why the mechano-luminescence was observed only in triclinic feldspars; (2) compression-induced transition from a modulated $P\bar{1}$ structure to $I\bar{1}$. This could explain the

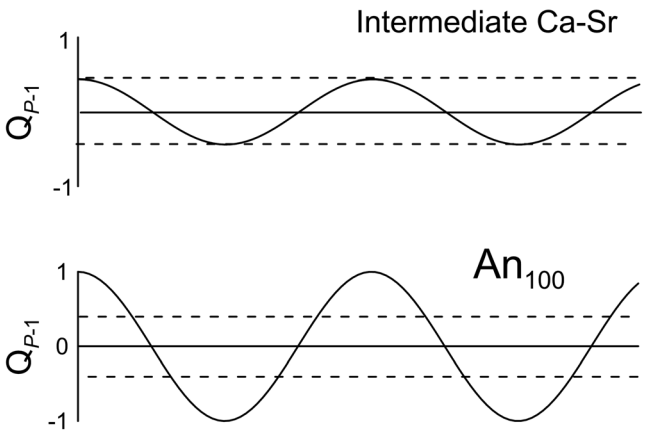

FIGURE 9 A possible model for the mechano-luminescence in Ca and Sr feldspars. The compression promotes the luminescence only for configurations close to the $I\bar{1}$ structure (between dashed lines). These are less common in anorthite, showing higher fluctuations, but can be enhanced by increasing Sr content and decreasing fluctuation amplitude, or by increasing pressure.

higher efficiency of $P\bar{1}$ intermediate configurations, which being closer to the transition than anorthite would require lower energy for their activation.

In Figure 9, a possible model for detrapping in intermediate modulated structures is shown. The modulations occur with local $P\bar{1}$ structures, more or less deformed, averaging a $I\bar{1}$ structure; the coexistence of different local structures accounts for the broadening in Raman spectra. The modulations can be described by fluctuations of a local structural parameter for the primitive structure ($Q_{P\bar{1}}$, not to be confused with that describing the deviation to a ferroelastic structure, Q_D). Assuming that the distribution of local configurations for Eu is similarly modulated, mechano-luminescence can occur in local structures close to the $I\bar{1}$ structure, which are activated by compression. These configurations close to the $I\bar{1}$ structure become more common as the amplitude of the fluctuations decreases, like in intermediate Ca and Sr feldspars, but disappear when the local structure becomes $I\bar{1}$.

4 | CONCLUSIONS

Raman spectra describe at a relatively short-range level the structure. We have found in Ca-Sr feldspars evidences of the transition between the $P\bar{1}$ and $I\bar{1}$ structures, in a change of hard mode peak positions at a composition between $An_{60}SrF_{40}$ and $An_{40}SrF_{60}$. At a long-range level, only the disappearance of few *c*-type faint diffractions in overexposed TEM patterns pinpoints the transition.

The Raman evidence for the ferro-elastic transition $I\bar{1}$ to $I2/c$ is scanty. The suggestion is that the ferroelastic transition at local level is related to a structural distortion of a configuration similar in the $I\bar{1}$ and $I2/c$ structure.

In terms of explaining the mechano-luminescence of intermediate compositions, we suggest that the mechano-luminescence in the $P\bar{1}$ structure, close to the transition, could be related to detrapping after a mechanically induced transition to $I\bar{1}$, and/or for feldspars which are already $I\bar{1}$, by detrapping the luminescent cations at the boundaries of the albite twins.

A different degree of Al-Si order does have an effect on this transition, in that it changes composition, temperature and pressure for the ferroelastic and the *P-I* phase transitions in $Ca_{1-x}Sr_xAl_2Si_2O_8$ feldspars.[5,9,11,36] The same occurs for the *P-I* transition in anorthite.[59] This could provide the basis for an improvement in the mechano-luminescence efficiency. Further investigation on cation order, phase transition and detrapping, analysing samples after different annealing, that is, different Al-Si cation order, could be a way to maximize the mechano-luminescence, for instance promoting highly disordered structure in feldspars with higher Ca content. Moreover, exchange of Ge for Si could have an effect on phase transitions and cation ordering, as previously observed in pyroxenes.[60,61]

Finally, the luminescence of feldspars has promising aspects also beyond material sciences. Anorthite can be a host for luminescence activators, even in very small amount. In an investigation on the CR2 Renazzo carbonaceous chondrite, the presence in anorthite of trace Cr, an element normally not present even as an impurity, could be detected by the analysis of the photoluminescence spectrum.[30] This is most effective when rare earth elements exchange with alkali-earth. For instance in Sr-feldspar doped with Eu^{3+} there are three main emission peaks at 578, 591 and 614 nm.[22]

The high temperature of formation of the Ca and Sr-feldspars, together with their easier exchange with rare earth elements due to the similar cation radius, make these phases a good host for rare earth. This could give a hint in the analysis of the luminescence in ceramics.[62]

ACKNOWLEDGEMENTS

The authors would like to thank Piera Benna for contributing to the synthesis of the samples and for providing us with them. Comments by the editor and three anonymous reviewer improved this paper. The Interdepartmental Center Giovanni Scansetti is thanked for the use of the micro-Raman spectrometer.

ORCID

Nadia Curetti https://orcid.org/0000-0002-6300-7133

REFERENCES

[1] A. Kyono, M. Kimata, *Miner. Mag.* **2001**, *65*(4), 523. https://doi.org/10.1180/002646101750377542
[2] P. Benna, E. Bruno, *Am. Miner.* **2001**, *86*(5–6), 690.
[3] N. Curetti, P. Benna, E. Bruno, *Am. Miner.* **2015**, *100*(7), 1568. https://doi.org/10.2138/am-2015-5000
[4] N. Curetti, P. Benna, E. Bruno, *Phys. Chem. Miner.* **2017**, *44*, 181. https://doi.org/10.1007/s00269-016-0847-0
[5] M. Tribaudino, P. Benna, E. Bruno, *Am. Miner.* **2000**, *85*, 963. https://doi.org/10.2138/am-2000-0710
[6] M. Tribaudino, P. Benna, F. Nestola, C. Meneghini, E. Bruno, *Phys. Chem. Miner.* **2005**, *32*, 314. https://doi.org/10.1007/s00269-005-0469-4
[7] H. U. Bambauer, H. E. Nager, N. Jb, *Miner. Abh.* **1981**, *141*, 225.
[8] M. D. McGuinn, S. A. T. Redfern, *Miner. Mag.* **1994**, *58*(390), 21. https://doi.org/10.1180/minmag.1994.058.390.02
[9] M. Tribaudino, P. Benna, E. Bruno, *Phys. Chem. Miner.* **1993**, *20*, 221.

[10] M. Tribaudino, P. Benna, E. Bruno, *Am. Miner.* **1995**, *80*, 907.
[11] M. Tribaudino, M. Zhang, E. K. H. Salje, *Miner. Mag.* **2009**, *73*, 119. https://doi.org/10.1180/minmag.2009.073.1.119
[12] P. Benna, E. Bruno, *Am. Miner.* **2003**, *88*(10), 1532. https://doi.org/10.2138/am-2003-1016
[13] P. Benna, F. Nestola, T. B. Ballaran, T. Balić-Žunić, L. F. Lundegaard, E. Bruno, *Am. Miner.* **2007**, *92*(7), 1190. https://doi.org/10.2138/am.2007.2402
[14] H. Mimura, T. Kanno, *J. Nucl. Sci. Technol.* **1985**, *22*(4), 284. https://doi.org/10.1080/18811248.1985.9735658
[15] H. Tang, X. Shu, W. Huang, Y. Miao, M. Shi, S. Chen, L. Bingsheng, L. Fen, X. Yi, S. Dadong, X. Lu, *J. of Hazard. Mat.* **2021**, *407*, 124761. https://doi.org/10.1016/j.jhazmat.2020.124761
[16] N. P. Bansal, C. H. Drummond III, *J. Am. Ceram. Soc.* **1993**, *76*(5), 1321. https://doi.org/10.1111/j.1151-2916.1993.tb03758.x
[17] P. Ptáček, F. Šoukal, T. Opravil, E. Bartoníčková, J. Wasserbauer, *Ceram. Int.* **2016**, *42*(7), 8170. https://doi.org/10.1016/j.ceramint.2016.02.024
[18] F. Clabau, A. Garcia, P. Bonville, D. Gonbeau, T. Le Mercier, P. Deniard, S. Jobic, *J. Solid State Chem.* **2008**, *181*(6), 1456. https://doi.org/10.1016/j.jssc.2008.03.011
[19] S. Ye, Z. S. Liu, X. T. Wang, J. G. Wang, L. X. Wang, X. P. Jing, *J. Lumin.* **2009**, *129*(1), 50. https://doi.org/10.1016/j.jlumin.2008.07.015
[20] S. Kubota, H. Yamane, M. Shimada, *Chem. Mater.* **2002**, *14*(10), 4015. https://doi.org/10.1021/cm025607o
[21] P. Ma, B. Yuan, Y. Sheng, K. Zheng, Y. Wang, C. Xu, Z. Haifeng, Y. Song, *J. Alloys Compd.* **2017**, *714*, 627. https://doi.org/10.1016/j.jallcom.2017.04.296
[22] X. Li, C. Yang, Q. Liu, X. Wang, X. Mi, *Ceram. Int.* **2020**, *46*(11) Part A, 17376. https://doi.org/10.1016/j.ceramint.2020.04.027
[23] Y. Wu, L. Zhu, H. Mao, *Ceram. Int.* **2018**, *44*(8), 10015. https://doi.org/10.1016/j.ceramint.2018.03.030
[24] W. Dai, J. Hu, G. Liu, S. Xu, K. Huang, J. Zhou, M. Xu, *J. Lumin.* **2020**, *217*, 116807. https://doi.org/10.1016/j.jlumin.2019.116807
[25] L. Zhang, H. Yamada, Y. Imai, C. N. Xu, *JES* **2008**, *155*(3), J63. https://doi.org/10.1149/1.2825141
[26] A. Feng, P. F. Smet, *Mater.* **2018**, *11*(4), 484. https://doi.org/10.3390/ma11040484
[27] L. Zhang, C.-N. Xu, H. Yamada, N. Bu, *J. Electrochem. Soc.* **2010**, *157*(3), J50. https://doi.org/10.1149/1.3274879
[28] H. Fang, G. Qiu, J. Li, X. Wang, *J. Alloys Compd.* **2018**, *763*, 267. https://doi.org/10.1016/j.jallcom.2018.05.294
[29] A. Feng, S. Michels, A. Lamberti, W. Van Paepegem, P. F. Smet, *Acta Mater.* **2020**, *183*, 493. https://doi.org/10.1016/j.actamat.2019.11.014
[30] M. Tribaudino, D. Bersani, L. Mantovani, M. Pizzati, G. Salviati, *J. Raman Spectrosc.* **2021**, *52*, 1892.
[31] B. H. Toby, R. B. Von Dreele, *J. Appl. Crystallogr.* **2013**, *46*(2), 544. https://doi.org/10.1107/S0021889813003531
[32] I. Aliatis, E. Lambruschi, L. Mantovani, D. Bersani, S. Andò, G. D. Gatta, P. Gentile, E. Salvioli-Mariani, M. Prencipe, M. Tribaudino, P. P. Lottici, *J. Raman Spectrosc.* **2015**, *46*, 501. https://doi.org/10.1002/jrs.4670
[33] P. Benna, M. Tribaudino, E. Bruno, *Phys. Chem. Miner.* **1995**, *22*, 343. https://doi.org/10.1007/BF00213330
[34] P. Benna, M. Tribaudino, E. Bruno, *Am. Miner.* **1996**, *81*(11–12), 1337. https://doi.org/10.2138/am-1996-11-1205
[35] W. Loewenstein, *Am. Mineral.* **1954**, *39*, 92.
[36] R. J. Angel, *Am. Miner.* **1992**, *77*(9–10), 923.
[37] M. Tribaudino, P. Benna, E. Bruno, *Am. Miner.* **1998**, *83*, 159.
[38] M. A. Carpenter, *Am. Miner.* **1991**, *76*(7–8), 1110.
[39] P. Németh, M. Tribaudino, E. Bruno, P. R. Buseck, *Am. Miner.* **2007**, *92*, 1080. https://doi.org/10.2138/am.2007.2504
[40] M. Tribaudino, R. J. Angel, F. Camara, F. Nestola, D. Pasqual, I. Margiolaki, *Contrib. Mineral. Petrol.* **2010**, *160*, 899. https://doi.org/10.1007/s00410-010-0513-3
[41] M. Tribaudino, R. J. Angel, *Phys. Chem. Miner.* **2012**, *39*, 699. https://doi.org/10.1007/s00269-012-0524-x
[42] A. Kremenovic, P. H. Colomban, B. Piriou, D. Massiot, P. Florian, *J. Phys. Chem. Solids* **2003**, *64*, 2253. https://doi.org/10.1016/S0022-3697(03)00252-X
[43] A. Kremenovic, P. Norby, R. Dimitrijevic, V. Dondur, *Solid State Ionics* **1997**, *101-103*, 611. https://doi.org/10.1016/S0167-2738(97)84091-X
[44] A. Kremenovic, P. Norby, R. Dimitrijevic, V. Dondur, *Phase Transitions* **2004**, *77*, 955. https://doi.org/10.1080/01411590412331282805
[45] D. A. McKeown, *Am. Miner.* **2005**, *90*, 1506. https://doi.org/10.2138/am.2005.1726
[46] D. Bersani, I. Aliatis, M. Tribaudino, L. Mantovani, A. Benisek, M. A. Carpenter, G. D. Gatta, P. P. Lottici, *J. Raman Spectrosc.* **2018**, *49*, 684. https://doi.org/10.1002/jrs.5340
[47] I. Daniel, P. Gillet, S. Ghose, *Am. Miner.* **1995**, *80*(5–6), 645. https://doi.org/10.2138/am-1995-7-804
[48] D. W. Matson, S. K. Sharma, J. A. Philpotts, *Am. Miner.* **1986**, *71*(5–6), 694.
[49] G. Van Tendeloo, S. Ghose, S. Amelinckx, *Phys. Chem. Minerals* **1989**, *16*, 311. https://doi.org/10.1007/BF00199550
[50] R. J. Angel, N. L. Ross, *Eos* **1988**, *69*, 498.
[51] P. H. Ribbe, H. D. Megaw, *Nor. J. Geol.* **1962**, *198*, 158.
[52] T. Echigo, M. Hoshino, M. Kimata, M. Shimizu, T. Matsui, N. Nishida, Z. Kristallogr, *Cryst. Mater.* **2014**, *229*(6), 435. https://doi.org/10.1515/zkri-2013-1713
[53] G. Chiari, M. Calleri, E. Bruno, P. H. Ribbe, *Am. Miner.* **1975**, *60*(1–2), 111.
[54] M. D. McGuinn, S. A. T. Redfern, *Am. Miner.* **1994**, *79*, 24.
[55] B. L. Phillips, M. D. McGulnn, S. A. Redfern, *Am. Miner.* **1997**, *82*(1–2), 1.
[56] P. Benna, E. Bruno, *Mineral. Mag.* **2006**, *70*(1), 65. https://doi.org/10.1180/0026461067010313
[57] M. A. Carpenter, E. K. H. Salje, *Mineral. Mag.* **1989**, *53*, 483. https://doi.org/10.1180/minmag.1989.053.372.09
[58] J. Töpel-Schadt, W. F. Müller, H. Pentinghaus, *J. Mater. Sci.* **1809**, *13*, 1978. https://doi.org/10.1007/BF00548745
[59] M.A. Carpenter, In I. Parsons, *Ed. Feldspars and Their Reactions, NATO ASI Series 421*, **1994**, 221–270 Springer, Dordrecht. https://doi.org/10.1007/978-94-011-1106-5_6
[60] E. Lambruschi, I. Aliatis, L. Mantovani, M. Tribaudino, D. Bersani, G. Redhammer, P. P. Lottici, *J. Raman Spectrosc.* **2015**, *46*, 586. https://doi.org/10.1002/jrs.4681

[61] M. Tribaudino, I. Aliatis, D. Bersani, G. D. Gatta, E. Lambruschi, L. Mantovani, G. Redhammer, P. P. Lottici, *J. Raman Spectrosc.* **2017**, *48*, 1443. https://doi.org/10.1002/jrs.5134

[62] P. Colomban, *Materials* **2022**, *15*(9), 3158.

SUPPORTING INFORMATION

Additional supporting information can be found online in the Supporting Information section at the end of this article.

How to cite this article: N. Curetti, D. Bernasconi, M. Tribaudino, *J Raman Spectrosc* **2024**, *55*(7), 833. https://doi.org/10.1002/jrs.6675